RESEARCH PAPERS

Acta Cryst. (1996). B52, 569–575

A Synchrotron X-ray Study of the Electron Density in Y_2BaCuO_5

R. HSU,[a]* E. N. MASLEN[a] AND N. ISHIZAWA[b]

[a]*Crystallography Centre, University of Western Australia, Nedlands 6009, Australia, and* [b]*Research Laboratory of Engineering Materials, Tokyo Institute of Technology, 4259 Nagatsuta, Midori-Ku, Yokohama 227, Japan. E-mail: rh@crystal.uwa.edu.au*

(*Received 17 July 1995; accepted 3 January 1996*)

Abstract

The deformation density ($\Delta\rho$) for Y_2BaCuO_5, barium diyttrium cuprate, determined by single-crystal X-ray diffraction with synchrotron radiation, is affected to only a limited degree by the bonding interactions involving the O anions. Electron density is strongly depleted along the cation–cation contacts within the mirror plane in the structure and is transferred to regions between mirror planes that do not lie along short cation–cation vectors. The structural geometry for the CuO_5 moiety, with the Cu atom in the +2 state, closely resembles that of the Cu_2O_5 group in $YBa_2Cu_3O_{7-\delta}$, for which the +3 state involvement for Cu has been suggested. Space group *Pnma*, orthorhombic, M_r = 458.68, a = 12.1793 (7), b = 5.6591 (5), c = 7.1323 (4) Å, V = 491.6 Å^3, Z = 4, D_x = 6.197 Mg m^{-3}, λ = 0.9 Å, $\mu_{0.9}$ = 28.893 mm^{-1}, $F(000)$ = 812, T = 293 K, R = 0.020, wR = 0.020, S = 3.09 (5) for 2225 unique reflections.

1. Introduction

To help explain the high-temperature superconductivity of $YBa_2Cu_3O_{7-\delta}$ (Bednorz & Mueller, 1986; Wu, Ashburn, Torng, Hor, Meng, Gao, Huang, Wang & Chu, 1987), Cava, Batlogg, van Dover, Murphy, Sunshine, Siegrist, Remeika, Rietman, Zahurak & Espinosa, (1987) studied the related semi-conducting greenish oxide Y_2BaCuO_5, which often occurs as an impurity (Weidinger, Budnick, Chamberland, Golnik, Niedermayer, Recknagel, Rossmanith & Yang, 1988). The magnetic ordering of Y_2BaCuO_5 at 15 K may be related to the superconducting phase transition in $YBa_2Cu_3O_{7-\delta}$.

Some hypotheses relate the high-temperature superconductivity of the 123 compound to the oxidation number of the Cu2 atom. Charge balance for the oxidation states of +2 for Ba, +3 for Y and −2 for O requires that Cu in Y_2BaCuO_5 be in a +2 state, whereas that for Cu2 in $YBa_2Cu_3O_{7-\delta}$ is frequently cited as exceeding +2 when δ falls below 0.5. Because Y_2BaCuO_5 is unaffected by non-stoichiometry or disorder, its structural geometry and $\Delta\rho$ topography provide reference standards with which those for Cu2 in $YBa_2Cu_3O_{7-\delta}$ can be compared.

An approximate X-ray powder diffraction structure analysis for Y_2BaCuO_5 by Michel & Raveau (1982) was confirmed by single-crystal X-ray diffraction (Hazen, Finger, Angel, Prewitt, Ross, Mao, Hadidiacos, Hor, Meng & Chu, 1987; Watkins, Fronczek, Wheelock, Goodrich, Hamilton & Johnson, 1988; Sato & Nakada, 1989). Distorted monocapped trigonal YO_7 prisms that share one triangular face form Y_2O_{11} blocks. The Ba^{2+} and Cu^{2+} cations lie in cavities in the three-dimensional edge-sharing network of Y_2O_{11} units. Each Ba atom is coordinated to 11 O atoms. The Cu atoms are located within distorted CuO_5 square pyramids. The low atom-site symmetries in these metal oxides allow their bonding and second nearest-neighbour interactions to be compared. This is more difficult for compounds where the bonding and second nearest-neighbour interactions have symmetry elements in common.

The electron density in Y_2BaCuO_5 single crystals was measured by Buttner & Maslen (1993) using Mo $K\alpha$ radiation. The $\Delta\rho$ topography near the Cu atom resembled that near Cu2 in $YBa_2Cu_3O_{7-\delta}$, which has similar coordination, but noise in that study made it difficult to draw firm conclusions on the longer range interactions that may be important in superconductivity. This noise can be reduced using synchrotron radiation.

2. Experimental

A crystal suitable for accurate diffraction imaging with sharp edges and well formed (10$\bar{1}$), (101), (010) and ($\bar{2}$01) faces was measured with a Philips 505 scanning electron microscope (SEM) at 1100 magnification to be 22.0 (3), 47.7 (3), 258.9 (3) and 17.0 (3) μm, respectively, from an internal origin. A bright red He–Ne laser beam (λ = 632.8 nm) grating calibration determined the 0.3 μm accuracy.

Intensity data were measured accurately at the Tsukuba Photon Factory by J. R. Hester, E. N.

Maslen and V. A. Streltsov, with the crystal mounted perpendicular to the (010) faces. The $\lambda = 0.9$ Å radiation from the beamline 14A vertical wiggler was polarized strongly in the vertical direction (Satow & Iitaka, 1989). A double-crystal monochromator with a double-focusing mirror is coincident with the equatorial plane of the four-circle diffractometer in a horizontal plane.

The diffraction profiles for five $h00$, four $0k0$ and three $00l$ reflections were essentially single peaks, except at the centres of the 400, 020 and 002 reflections, for which the NaI scintillation counter's linear range of 20 000 counts s^{-1} was exceeded so markedly that their profiles had double peaks. An attenuator, introduced automatically during data collection when the peak count rate exceeded a preset value, reduced strong intensities by the attenuation factor of 34.0 to within the range for which analytical dead time corrections were reliable.

Cell dimensions were determined from measured angles for six reflections ($79.0 < 2\theta < 105.3°$). The crystal was re-oriented during data collection when the intensities of standard reflections dropped suddenly by more than 10%, presumably because seismic activity disturbed the alignment.

Absorption corrections were evaluated by the analytical method (Alcock, 1974) with an attenuation coefficient calculated from atomic μ/ρ values for $\lambda = 0.9$ Å kindly updated by Creagh (1992). The crystal's elongated, mildly non-centrosymmetric shape was a critical test of the analytical absorption routine's precision. Optical path lengths calculated for some Friedel pairs differed initially, although equality was expected. Close scrutiny of the algorithm for forming Howell's polyhedra after analysing asymptotic forms for the optical path lengths using Mathematica (Wolfram, 1991) allowed the problems to be rectified. The precision of the *Xtal*3.2 system *ABSOR*B subroutine (Hall, Flack & Stewart, 1992) was improved to meet the needs of these calculations.

Secondary extinction corrections to $|F|^2$ based on Zachariasen's (1967) formalism as applied by Larson (1970) were first assessed by relating intensity differences for symmetry-related reflections to their diffraction path lengths (Spadaccini & du Boulay, 1992). The isotropic Zachariasen extinction coefficient r^* indicated was slightly negative and not significant. Extinction corrections of the F values for the unique reflections, optimized concurrently with the structural parameters by minimizing the disagreement between observed and calculated structure factors by least-squares, were also insignificant. These extinction corrections have the disadvantage of depending on the structural model used to evaluate F_c.

All calculations utilized the *Xtal*3.2 system installed on a DECstation 5000/120 computer. The Lorentz and polarization corrections applied assume the double-crystal monochromator to be perfect. The incident beam polarization factor for a 2θ monochromator angle of 16.57° was 0.9508. Atomic form factors were from *International Tables for X-ray Crystallography* (1974, Vol. IV). The structure-factor calculations included the $\Delta f'$, $\Delta f''$ values −1.346, 0.776 for Y, −0.063, 3.450 for Ba, 0.123, 1.943 for Cu and 0.018, 0.010 for O at 0.9 Å, kindly evaluated by Creagh (1992).

Full-matrix least-squares refinement minimized the residual $\Sigma w_i(|F_o| - |F_c|)^2$ with $w_i = 1/\sigma^2(F)$. The accuracy of the weak reflections, with $F_o < 10\sigma$ for only

Table 1. *Experimental details*

Crystal data	
Chemical formula	Y_2BaCuO_5
Chemical formula weight	458.68
Cell setting	Orthorhombic
Space group	*Pnma*
a (Å)	12.1793 (7)
b (Å)	5.6591 (5)
c (Å)	7.1323 (4)
V (Å^3)	491.59 (6)
Z	4
D_x (Mg m^{-3})	6.197
Radiation type	Synchrotron
Wavelength (Å)	0.9000 (1)
No. of reflections for cell parameters	6
θ range (°)	39.510–52.668
μ (mm^{-1})	28.893
Temperature (K)	293
Crystal form	Needle-like
Crystal size (mm)	0.0518 (3) × 0.0095 (3) × 0.0034 (3)
Crystal colour	Green
Data collection	
Diffractometer	Tsukuba
Data collection method	$\omega/2\theta$
Scan speed (° min^{-1})	16
Peak scan width; a + $b$tan θ (°)	0.40; 0.00
$(\sin\theta/\lambda)_{max}$	1.01
Absorption correction	Analytical
T_{min}	0.55
T_{max}	0.83
No. of measured reflections	16 154
No. of independent reflections	2415
No. of observed reflections	2225
Criterion for observed reflections	$F > \sigma(F)$
R_{int}	0.032
θ_{max} (°)	64.95
Range of h, k, l	$-24 \rightarrow h \rightarrow 24$ $-11 \rightarrow k \rightarrow 11$ $-14 \rightarrow l \rightarrow 14$
No. of standard reflections	6
Frequency of standard reflections	Every 100 reflections
Intensity decay (%)	10
Refinement	
Refinement on	F
R	0.020
wR	0.020
S	3.092
No. of reflections used in refinement	2233
No. of parameters used	49
H-atom treatment	H-atom parameters not refined
Weighting scheme	$w = 1/\sigma^2(F)$
$(\Delta/\sigma)_{max}$	0.00001
$\Delta\rho_{max}$ (e Å^{-3})	1.504
$\Delta\rho_{min}$ (e Å^{-3})	−5.234
Extinction method	None
Source of atomic scattering factors	*International Tables for X-ray Crystallography* (1974, Vol IV, Tables 2.2B and 2.3.1)

Table 2. *Positional and anisotropic vibration parameters ($Å^2 \times 10^5$) for Y_2BaCuO_5*

$U_{eq}(1/3)\sum_i\sum_j U_{ij}\,a_i^*\,a_j^*\,\mathbf{a}_i.\mathbf{a}_j$.

	x	y	z	U_{eq}	U_{11}	U_{22}	U_{33}	U_{12}	U_{13}	U_{23}
Y1	0.57388 (2)	0.75	1.10416 (3)	371 (7)	351 (6)	408 (7)	352 (6)	0	−7 (5)	0
Y2	0.78823 (2)	0.75	0.38365 (3)	366 (7)	339 (6)	393 (7)	365 (6)	0	−3 (5)	0
Ba	0.90483 (1)	0.75	−0.06980 (2)	684 (5)	599 (4)	638 (5)	816 (5)	0	−88 (4)	0
Cu	0.65941 (2)	0.75	0.71268 (4)	426 (10)	438 (9)	397 (9)	442 (9)	0	112 (7)	0
O1	0.5675 (1)	0.5072 (2)	0.8345 (2)	599 (42)	523 (36)	510 (42)	765 (39)	−62 (30)	66 (29)	69 (31)
O2	0.7724 (1)	0.5044 (2)	0.6438 (2)	724 (44)	783 (40)	642 (44)	748 (41)	251 (32)	231 (31)	230 (32)
O3	0.6004 (1)	0.75	0.4199 (2)	669 (60)	529 (51)	1012 (66)	465 (50)	0	11 (41)	0

5% of the extensive data, is reflected in low refinement indices, listed in Table 1.*

The refined atomic positions listed in Table 2 are fully consistent with those by Michel & Raveau (1982), Watkins *et al.* (1988), Sato & Nakada (1989), Hunter, Town, Davis, Russel & Taylor (1989), Pei, Paulikas, Veal & Jorgensen (1990), Salinas-Sanchez, Garcia-Munoz, Rodriguez-Carvajal, Saez-Puche & Martinez (1992) and Buttner & Maslen (1993). The vibration amplitudes in Table 2 do not show the anomalously low values for Y1 and Y2 reported by Watkins *et al.* (1988), being smaller than but closer to those in the X-ray tube study by Buttner & Maslen (1993). The vibration amplitudes resemble those for Ba, Y and Cu2 in the high-T_c compound in so far as Ba is relatively labile, Y is tightly bound and Cu shows intermediate behaviour.

3. Structural geometry

The cation coordinates chosen define a near linear Y1···Cu···Y2···Ba sequence, coplanar with O3 in the mirror plane at y = 0.75. All O atoms are near Cu, with O1 and O2 displaced below that mirror plane. Table 3 lists important interaction distances. The five-coordinated Cu atom has two Cu—O1, 1.974 (1) Å, and two Cu—O2, 2.016 (1) Å, bonds. The Cu—O3, 2.208 (2) Å, bond lies on the y = 0.75 mirror plane. The CuO_5 geometry resembles that around the Cu2 atom in the 123 superconducting phase (Buttner, Maslen & Spadaccini, 1992), as shown in Fig. 1. The elongated pyramid in Y_2BaCuO_5 is less distorted, with the Cu atom displaced by only 0.2268 Å from the oxygen base. The Cu—O1 and Cu—O2 bonds are tilted from the ideal octahedral orientation by 6.6 and 6.5°, respectively, which are smaller than the 7.7° for Cu2—O2 and Cu2—O3 in $YBa_2Cu_3O_{7-\delta}$ (Buttner *et al.*, 1992).

An isolated Cu^{2+} atom in an octahedral ligand field is unstable against small perturbations, because its d^9 state is degenerate, as predicted by the Jahn–Teller (Jahn & Teller, 1937) theorem. Thus, the CuO structure contains elongated O-atom octahedra with Cu at the centre (Langford & Louer, 1991). The common D_{4h} distortion to the Cu^{2+} atoms' symmetry has one axis pair of the octahedron elongated. The other two pairs are contracted. The structural geometry of the Cu atom in Y_2BaCuO_5 is roughly of this type. The pyramid base formed by four coplanar O1 and O2 atoms is not quite orthogonal to the Cu—O3 vector that defines the pyramid vertex.

The apical Cu—O distance is larger than those at the pyramid base due to the Jahn–Teller distortion normally associated with Cu^{2+} (Hewat, Fischer, Kaldis, Hewat, Jilek, Karpinski & Rusiecki, 1990). On the other hand,

Table 3. *Selected interaction-vector lengths and O—M—O′ angles for Y_2BaCuO_5*

M is Ba, Y1, Y2 or Cu, with O and O′ symmetry-related by reflection across the mirror plane at y = 0.75.

	Coordination		Interaction length (Å) *M*—O		Angle (°) O—*M*—O′	
Y1	7	$Y1^{i}$—O3	2.275 (2)		0 (on mirror)	
		Y^{ii}—$O1^{iii}$	2.296 (1)	×2	O1—Y1—O1	78.66 (5)
		Y^{iv}—$O1^{v}$	2.365 (1)	×2	O1—Y1—O1	71.04 (5)
		$Y1^{vi}$—$O2^{vii}$	2.379 (1)	×2	O2—Y1—O2	74.49 (5)
Y2	7	$Y2^{iv}$—O3	2.302 (2)		0 (on mirror)	
		$Y2^{viii}$—$O1^{ix}$	2.309 (1)	×2	O1—Y2—O1	78.16 (5)
		$Y2^{iv}$—$O2^{v}$	2.326 (1)	×2	O2—Y2—O2	73.37 (5)
		$Y2^{viii}$—$O2^{ix}$	2.355 (1)	×2	O2—Y2—O2	75.39 (5)
Ba	11	Ba^{x}—O3	2.611 (1)		0 (on mirror)	
		Ba^{viii}—$O3^{ix}$	2.8312 (3)	×2	O3—Ba—O3	176.05 (5)
		Ba^{xi}—$O2^{xii}$	2.951 (1)	×2	O2—Ba—O2	56.19 (4)
		Ba^{vii}—$O2^{ix}$	3.008 (1)	×2	O2—Ba—O2	57.19 (4)
		Ba^{v}—O^{xiii}	3.062 (1)	×2	O1—Ba—O1	53.34 (4)
		Ba^{vii}—$O1^{viii}$	3.248 (1)	×2	O1—Ba—O1	53.23 (4)
Cu	5	Cu^{iv}—O3	2.208 (2)		0 (on mirror)	
		Cu^{iv}—$O1^{v}$	1.974 (1)	×2	O1—Cu—O1	88.23 (5)
		Cu^{iv}—$O2^{v}$	2.016 (1)	×2	O2—Cu—O2	87.14 (5)

M—*M* contacts (< 5 Å)

	Y1	Y2	Ba	Cu
Y1	3.6678 (3) ×2	3.2846 (3)*	3.6717 (3) ×2	2.9801 (4)*
		3.4801 (3)*	3.9076 (3)*	4.2174 (3) ×2
		3.6469 (3) ×2	4.2173 (3)	4.3769 (3) ×2
			4.3318 (3)*	4.4635 (4)*
Y2		4.6466 (3) ×4	3.5321 (3)*	2.8230 (4)*
			3.6939 (3) ×2	3.1464 (3) ×2
			1.1488 (3)*	
			4.8547 (4)*	
Ba			3.7911 (2) ×2	3.2638 (4)*
				3.3676 (4)*
				3.5606 (3) ×2

Symmetry codes: (i) $x, y, 1+z$; (ii) $1-x, \frac{1}{2}+y, 2-z$; (iii) $1-x, 1-y, 2-z$; (iv) x, y, z; (v) $x, \frac{3}{2}-y, z$; (vi) $\frac{3}{2}-x, 1-y, \frac{1}{2}+z$; (vii) $\frac{3}{2}-x, \frac{1}{2}+y, \frac{1}{2}+z$; (viii) $\frac{3}{2}-x, 1-y, z-\frac{1}{2}$; (ix) $\frac{5}{2}-x, \frac{1}{2}+y, z-\frac{1}{2}$; (x) $\frac{1}{2}+x, \frac{3}{2}-y, \frac{1}{2}-z$; (xi) $x, y, z-1$; (xii) $x, \frac{3}{2}-y, z-1$; (xiii) $\frac{1}{2}+x, y, \frac{1}{2}-z$. * *M*—*M* contacts are within the same y layer.

* A list of structure factors has been deposited with the IUCr (Reference: AS0699). Copies may be obtained through The Managing Editor, International Union of Crystallography, 5 Abbey Square, Chester CH1 2HU, England.

one would expect a Jahn–Teller distorted Cu^{2+} atom to occupy a larger volume than a Cu^{3+} atom that is not Jahn–Teller distorted. Formal charge balance requires Cu in Y_2BaCuO_5 to be divalent. It is most unlikely to be in a mixed-valence state. From the data in Fig. 1 it is readily shown that the volume of the CuO_5 pyramid in Y_2BaCuO_5 is slightly smaller than that of the $Cu2O_5$ pyramid in $YBa_2Cu_3O_{7-\delta}$. Vibrational data do not indicate that the latter group is anomalous, in any sense. The similarity of the Cu2 atom in $YBa_2Cu_3O_{7-\delta}$ to that indicated for the Cu atom in Y_2BaCuO_5 by this accurate analysis argues against the hypothesis that the former atom is in a 3+ state.

The O1···O1, O1···O2 and O2···O2 distances of 2.748 (2), 2.842 (1) and 2.779 (2) Å, respectively, are comparable to the O···O 2.766 Å distances in the TiO_6 octahedra for $SrTiO_3$ (Buttner & Maslen, 1992). To first order, O1 and O2 behave as if they are in close non-bonded contact. The longer O1···O3 and O2···O3 distances of 3.285 (2) and 2.977 (1) Å raise the possibility that the cations play a significant role in defining the structural framework for Y_2BaCuO_5.

An approximate mirror line within the mirror plane at y = 0.75 connects Ba atoms separated by the c dimension, as shown in Fig. 2. The Ba atom is located on the pseudo-mirror line, the linear sequences Y1···Cu···Y2···Ba on both sides being related by the approximate mirror. That mirror is broken by O3. Off the exact mirror plane the approximate mirror persists as far as the closest O1, O2 pair. As seen from the atom coordinates projected onto the plane of Fig. 2, the deviation from symmetry is due to non-equivalence of O3 on one side to an O2 pair on the other.

The BaO bond strengths, indicated by their length, are affected by the number and strength of competing bonds to other cations. The Ba atom bonds tightly only to O3. There is a Ba—O3 bond, 2.611 (1) Å, on the y = 0.75 mirror plane and two m-related bonds of 2.8312 (3) Å. The O3 atom's apical bond to Cu is correspondingly weak, whereas O1 and O2 form strong Cu—O bonds.

The coordination geometries for both Y1 and Y2 correspond one to one, Y—O3 being the shortest Y—O bond in each case. Each YO_7 coordination polyhedron in Y_2BaCuO_5 contains two mirror-related O1 atoms and an O3 atom, almost co-planar with the Y atom. The other two pairs of mirror-related O atoms complete the sevenfold Y-atom coordination.

In general, the contact distances indicate crowding of the Y cations in the mirror plane at y = 0.75. Thus, the Cu···Y2 vector, 2.8230 (4) Å, lies in the mirror plane, whereas the shortest Cu···Y2 vector between adjacent layers is 3.1464 (3) Å. The Y1···Y2, 3.2846 (3) Å, and Ba···Y1 contacts, 3.9076 (3) Å, are contracted by O3 involvement. The situation for the Ba atom is not clear cut. The shorter Ba···Cu contacts 3.2638 (4) and 3.3676 (4) Å lie in the y = 0.75 plane, the former being contracted by interactions involving O3. On the other hand, the interplane Ba···Y2, 3.5321 (3) Å, vector is shorter than the in-plane Ba···Y1, 3.9076 (3) Å, vector, because Y2 is dragged towards Ba by the Y2—O1 and Y2—O2 interactions.

4. Atomic vibrations

Atomic vibrations are relevant here as indicators of the strengths of interactions. In general, the vibrational data are consistent with the view that the cations' motions are limited by strong M—O bonding, but all of the data are consistent with the hypothesis that such motions are also impeded appreciably by the stronger cation–cation interactions.

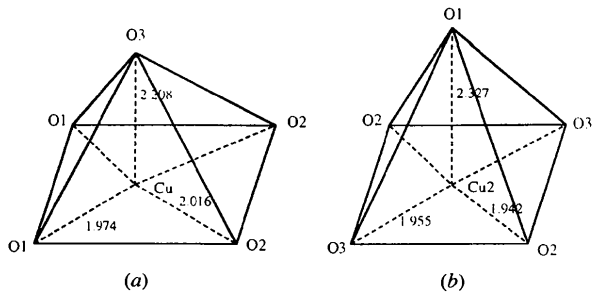

(a) (b)

Fig. 1. Structural geometry of Cu pyramid (values in Å): (a) Y_2BaCuO_5; (b) the superconducting phase $YBa_2Cu_3O_{7-\delta}$.

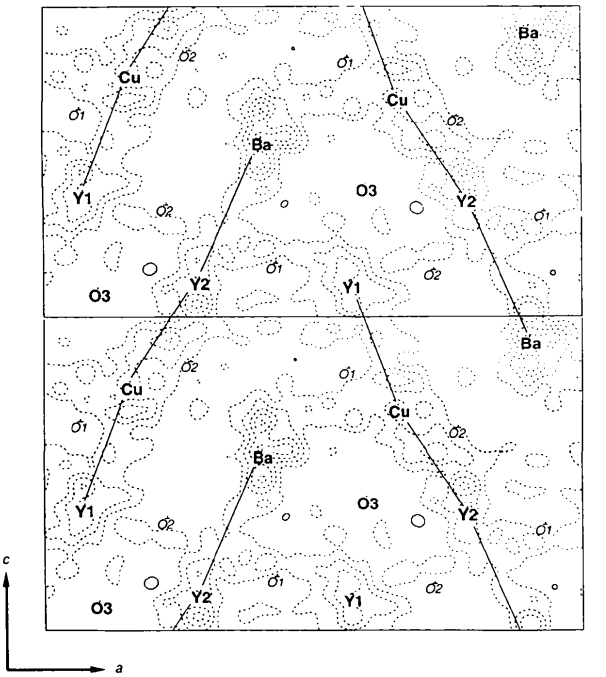

Fig. 2. $\Delta\rho$ in the (010) plane, y = 0.75, of Y_2BaCuO_5. Map borders 12.2 × 7.2 Å. Contour intervals 1.0 e $Å^{-3}$; positive and negative contours are represented by solid lines and dashes, respectively.

Table 4. *Atomic charges based on Hirshfeld partitioning of* $\Delta\rho$

Atom	Charge (e)	Atom	Charge (e)
Y1	2.3 (1)	O1	−1.7 (1)
Y2	2.0 (1)	O2	−1.8 (1)
Ba	1.7 (1)	O3	−1.7 (1)
Cu	1.8 (1)		

The largest Cu-atom vibration is *ca* 45° from both the *a* and *c* axes, creating angles of 15.9° to the O4 plane normal and 71.7° to the Y1···Cu···Y2 line, suggesting that both the Cu—O bonds and the Cu···Y contacts restrict the Cu-atom vibrations.

The O1-atom motion is closer to isotropic than those of O2 and O3.

The coordination of the Cu and Y atoms around O1 is approximately tetrahedral, neglecting the weaker Ba—O1 interactions. The O1 atom's larger U_{33} element can be attributed to a modest flattening of the tetrahedron in the *c* direction. The coordination of the Cu and Y atoms around O2 is closer to square planar. The O2 atom has its largest motion along Ba—O2 contacts normal to that plane. The coordination of O3 with Cu, two Y atoms and the nearest Ba atom is also square planar. Its large U_{22} vibration, being normal to the $y = 0.75$ plane, indicates that O3 vibrates maximally roughly along the two *m*-related Ba—O3 2.831 Å vectors.

As O1 and O2 atoms are not pinned tightly at the corners of the O4 plane, the CuO_4 moiety oscillates about the normal plane. As U_{ij} for O1 are less than those for O2, the centre of rotation passes not through the central Cu atom itself, but nearer to O1 than to O2.

The Ba atom is packed more loosely than Cu, as indicated by its larger U_{eq} value listed in Table 2. If the Ba—O3 bond were very strong we should expect the minimum Ba-atom vibration along that bond, whereas the minimum vibration eigenvector makes an angle of 43.3° with the Ba—O3 vector. It is closer to the shortest Ba···Cu interaction and almost normal to the Y2···Cu···Y1 sequence, indicating that Ba···cation interactions restrict the Ba-atom vibrations.

Tight packing results in the low vibrational parameters for both Y atoms listed in Table 2. The mean Y—O bond length of 2.326 Å for Y2, which has the lower U_{eq} value, compares with 2.336 Å for Y1. However, Y—O bond lengths are not necessarily decisive, since Y2 is also involved in the shorter $M\cdots M'$ contacts with both Ba and Cu. Both Y atoms vibrate maximally along the *b* axis, but the anisotropy is less marked for Y2, which makes Y2···Cu contacts of 3.1464 (3) Å in the [010] direction. There is no similarly directed Y1···cation vector.

The Y1 motion in the *xz* plane is almost isotropic, as is consistent with having its three shortest Y—O bonds almost at right angles. The Y2 atom vibrates least strongly along the Y2—O3 bond, which is almost coplanar with the two short Y2—O1 bonds. However, the degree of anisotropy of its motion in the *xz* plane is mild and its interactions with Cu and Y1 in that plane may dampen its motion in the *c* direction. The O-atom vibration ellipsoids generally show hardness along the Y—O bond directions and softness perpendicular to those bonds, except for Y1—O1, 2.365 (1), and Y2—O1, 2.309 (1) Å, for which such softness may be precluded by other Y—O1 or Cu—O1 interactions.

5. Atomic charges

Atomic charges, determined by projecting the difference density $\Delta\rho$ onto atomic density basis functions following the method of Hirshfeld (1977), are listed in Table 4. There is close agreement between the charges for O1, O2 and O3, and, to a lesser degree, between those for Y1 and Y2. The O-atom charges are far more consistent than values determined earlier with Mo $K\alpha$ radiation (Buttner & Maslen, 1993).

The O-atom values are reasonable for atoms formally in 2^- states. The Cu-atom charge of +1.8 (1) e is likewise reasonable for a Cu^{II} atom that overlaps strongly with its neighbours, as is indicated by its low U_{ij} values. Crowding of atoms is associated with strong exchange depletion of the electron density and consequently with the development of a positive charge. The comparatively low positive charge of +1.7 e for the loosely bonded Ba atom is consistent with it having larger vibration amplitudes than the other cations. This reflects less transfer of valence electron density from cation to anion by exchange depletion. The higher charges on Y1 and Y2 are consistent with their lower vibration amplitudes, although it might also be argued that these reflect the higher oxidation states for the Y cations.

6. Difference density

Difference density ($\Delta\rho$) maps based on the structure model in Table 2 with free-atom-scattering factors were evaluated. Electron density is transferred from the tightly packed regions of the structure, shown in Fig. 2, to form a lumpy sea in the space between the mirror planes at $y = 0.25$ and 0.75. The gradient of positive $\Delta\rho$ is low everywhere, *i.e.* the electron sea between the mirror planes is slowly varying. The major $\Delta\rho$ features do not have a simple relationship to the nearest-neighbour geometry. The complex $\Delta\rho$ topography suggests that the ligand field has significant contributions from both nearest- and second nearest-neighbour interactions.

Density is depleted most strongly along the shorter second nearest-neighbour cation–cation vectors. This is consistent with exchange depletion of valence electrons that overlap with closed electron sub-shells in the cations. There is very little positive $\Delta\rho$ on the $y = 0.75$ section, or equivalently at $y = 0.25$, on which all cations and the O3 atom are packed tightly. The density at the

O3 site is close to zero. The featureless $\Delta\rho$ topography near this site contrasts with that nearer the cations.

Electron density is depleted especially along the sequence of short cation–cation contacts Y1···Cu···Y2···Ba. There are weaker depletions near the Y1···Y2 and the two symmetry-independent Cu···Ba vectors, forming cross-links between the Y1···Cu···Y2···Ba lines. Atoms in these lines are cross-linked by connections zigzagging along the *a* axis. The Ba atom is on a pseudo-mirror line. Electron depletion between cations is broken at Ba···Y1, because of O3 involvement, as shown in Fig. 2. The deviation from symmetry is due to the non-equivalence of O3, on one side, to an O2 pair on the other.

Four second nearest-neighbour cations surround the Cu atom in the y = 0.75 plane. Proceeding from the Cu—O3 bond in a clockwise direction: Cu···Ba 3.2638 (4), Cu···Y1 2.9801 (4), Cu···Ba 3.3676 (4) and Cu···Y2 2.8230 (4) Å. Depletion is more pronounced along the Cu···Y1, Cu···Y2 and shorter Cu···Ba contacts. The two Ba and two Y atoms surrounding Cu are in approximately symmetric arrangements. Deviations from symmetry are due to the non-equivalence of O3, on one side, to the O1 pair and O2 pair on the other.

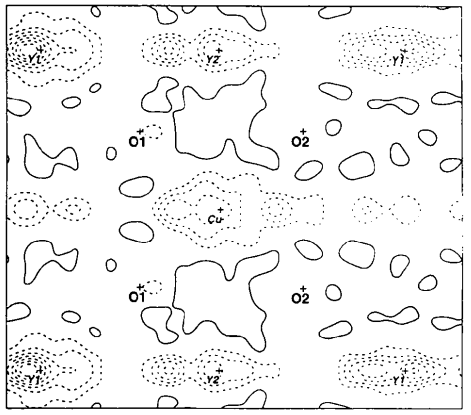

(*a*) O4 plane

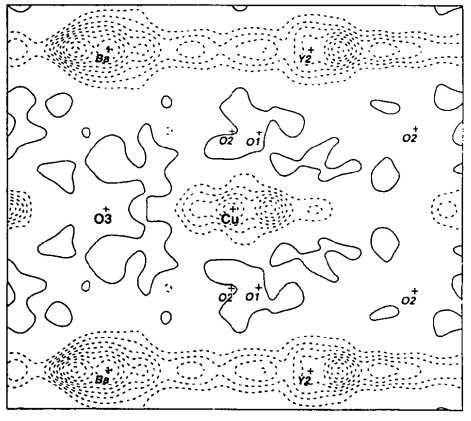

(*b*) Cu—O3 2.208 (2) Å

Fig. 3. $\Delta\rho$ sections perpendicular to the (010) plane for Y_2BaCuO_5: (*a*) through O—O contacts in CuO_5; (*b*) through Cu—O bonds. Map borders 7.9 × 7.1 Å, contour intervals 0.5 e Å^{-3}; positive and negative contours are represented by solid lines and dashes, respectively.

Four local minima surround the Cu nucleus; there is a -2.9 e Å^{-3} minimum at the intersection of the O1···O3···O1 plane and the Cu···Ba vector, displaced 1.02 Å from the Cu nucleus; a -3.7 e Å^{-3} hole, displaced 0.65 Å along the c axis, is tilted by 21° from the Cu···Y1 vector; another -1.3 e Å^{-3} minimum in the O1···O2···O2···O1 plane is displaced 0.6 Å from the Cu nucleus; and the fourth, -4.0 e Å^{-3} deep, 1.32 Å from the Cu nucleus in the O2···O3···O2 plane, is tilted 6° from the Cu···Y2 vector. Where such minima in the y = 0.75 plane are not aligned accurately along cation–cation vectors, the topography can be interpreted in terms of movement of the depletion away from O3, that is of density towards that atom. To a minor extent, the O anion influences the deformation density.

Fig. 3(*a*), a $\Delta\rho$ section perpendicular to the (010) plane through the O1···O2···O2···O1 contacts, shows that electrons accumulate along the O1···O2 contacts. Less deformation density accumulates around O1, which from U_{ij} moves less than O2.

The $\Delta\rho$ section perpendicular to the (010) plane passing through the Cu—O3 bond in Fig. 3(*b*) shows that the slowly varying electron sea between the mirror planes accumulates along all the O···O contacts. The approximately symmetric $\Delta\rho$ topography around the Cu nucleus might have been expected from the characteristics of *s*- and *d*-valence electron orbitals for this atom. An electron valley, of 3.5606 (3) Å, links Cu at y = 0.75 with Ba at y = 0.25. The corresponding valley along the Cu···Y2 vector exists, but is less prominent.

The ligand field energy for the 3*d* group of elements is larger than the spin-orbit coupling. The pure 3*d* states are split by such a field into a lower triplet t_{2g} and upper doublet e_g (Abraham & Bleaney, 1970). Fig. 3(*a*) shows that the electron density does deplete near the Cu atom along the Cu—O1 and Cu—O2 vectors. Well defined depletions on either side of the Cu nucleus along the line of the Cu—O3 vector also occur, as shown in Fig. 3(*b*). One could argue that these represent the e_g orbital depletions expected for a Cu^{2+} atom, but as seen from Fig. 2 they relate more closely to the second nearest-neighbour Cu···*M* interactions than to the Cu—O bonds. As the e_g orbitals are depleted one might expect that density would concentrate in the corresponding t_{2g} states. This is harder to identify in the $\Delta\rho$ map, but mild t_{2g} concentration could be masked by other contributions.

This work was supported by the Australian Research Council. Financial support of the Australian National Beamline Facility (ANBF) is also acknowledged. The

ANBF is funded by a consortium comprising the ARC, DITARD, ANSTO, CSIRO, ANU and UNSW. We are also indebted to Dr D. C. Creagh for his calculations of absorption coefficients and dispersions corrections.

References

Abraham, A. & Bleaney, B. (1970). *Electron Paramagnetic Resonance of Transition Ions*, pp. 365–490. Oxford: Clarendon Press.

Alcock, N. W. (1974). *Acta Cryst.* A**30**, 332–335.

Bednorz, J. G. & Mueller, K. A. (1986). *Z. Phys. B*, **64**, 189–193.

Buttner, R. H. & Maslen, E. N. (1992). *Acta Cryst.* B**48**, 639–644.

Buttner, R. H. & Maslen, E. N. (1993). *Acta Cryst.* B**49**, 62–66.

Buttner, R. H., Maslen, E. N. & Spadaccini, N. (1992). *Acta Cryst.* B**48**, 21–30.

Cava, R. J., Batlogg, B., van Dover, R. B., Murphy, D. W., Sunshine, S., Siegrist, T., Remeika, J. P., Rietman, B. A., Zahurak, S. & Espinosa, G. P. (1987). *Phys. Rev. Lett.* **58**, 1676–1679.

Creagh, D. C. (1992). Private communication.

Hall, S. R., Flack, H. D. & Stewart, J. M. (1992). Editors. *Xtal*3.2 *User's Guide and Reference Manual*. Universities of Western Australia, Australia, and Maryland, USA.

Hazen, R. M., Finger, L. W., Angel, R. J., Prewitt, C. T., Ross, N. L., Mao, H. K., Hadidiacos, C. G., Hor, P. H., Meng, R. L. & Chu, C. W. (1987). *Phys. Rev. B*, **35**, 7238–7240.

Hewat, A. W., Fischer, P., Kaldis, E., Hewat, E. A., Jilek, E., Karpinski, J. & Rusiecki, S. (1990). *J. Less-Common Met.* **164/165**, 39–49.

Hirshfeld, F. L. (1977). *Isr. J. Chem.* **16**, 198–201.

Hunter, B. A., Town, S. L., Davis, R. L., Russel, G. J. & Taylor, K. N. R. (1989). *Phys. C*, **161**, 594–597.

Jahn, H. A. & Teller, E. (1937). *Proc. R. Soc. London Ser. A*, **161**, 220–235.

Langford, J. I. & Louer, D. (1991). *J. Appl. Cryst.* **24**, 149–155.

Larson, A. C. (1970). *Crystallographic Computing*, edited by F. R. Ahmed, S. R. Hall & C. P. Huber, pp. 291–294. Copenhagen: Munksgaard.

Michel, C. & Raveau, B. (1982). *J. Solid State Chem.* **43**, 73–80.

Pei, S., Paulikas, A. P., Veal, B. W. & Jorgensen, J. D. (1990). *Acta Cryst.* C**46**, 1986–1988.

Salinas-Sanchez, A., Garcia-Munoz, J. L., Rodriguez-Carvajal, J., Saez-Puche, R. & Martinez, J. L. (1992). *J. Solid State Chem.* **100**, 201–211.

Sato, S. & Nakada, I. (1989). *Acta Cryst.* C**45**, 523–525.

Satow, Y. & Iitaka, Y. (1989). *Rev. Sci. Instrum.* **60**, 2390–2393.

Spadaccini, N. & du Boulay, D. (1992). *Xtal*3.2 *Reference Manual*, edited by S. R. Hall, H. D. Flack & J. M. Stewart, pp. 316–320. Universities of Western Australia, Australia, and Maryland, USA.

Watkins, S. F., Fronczek, F. R., Wheelock, K. S., Goodrich, R. G., Hamilton, W. O. & Johnson, W. W. (1988). *Acta Cryst.* C**44**, 3–6.

Weidinger, A., Budnick, J. I., Chamberland, B., Golnik, A., Niedermayer, C., Recknagel, E., Rossmanith, M. & Yang, D. P. (1988). *Phys. C*, 153–155, 168–169.

Wolfram, S. (1991). *Mathematica*, 2nd ed. California: Addison-Wesley.

Wu, M. K., Ashburn, J. R., Torng, C. J., Hor, P. H., Meng, R. L., Gao, L., Huang, Z. J., Wang, H. Q. & Chu, C. W. (1987). *Phys. Rev. Lett.* **58**, 908–910.

Zachariasen, W. H. (1967). *Acta Cryst.* A**23**, 558–564.